FLUTTER ASSESSMENT OF A ROTOR BLADE IN STEADY AXIAL FLIGHT BASED ON INDICIAL AERODYNAMICS

Jürgen Arnold, Juergen.Arnold@dlr.de, DLR German Aerospace Center (Germany)

Abstract

The 7AD rotor blade is assessed for flutter stability in steady axial flight. For the aeroelastic analyses, the multibody model is tightly-coupled with an unsteady aerodynamic model based on the extended Wagner function and related enhancements for the general motion of an airfoil section considering heave and pitch. The mathematical setup of the extended Wagner function in state space considers unsteady aerodynamic contributions related to the blade airfoil as well as rotor inflow and wake periodicity for axial flow in hover flight. A correction for the effective rotor inflow in climb and descent extends the applicability to steady axial flight. As known for articulated rotor blades, also the straight 7AD blade with parabolic blade tip shows the classical bending-torsion coupling which remains for all studied axial flight velocities. According results for climb and descent are evaluated in terms of a relative flutter onset taking hover as reference into account. Within the studied range of climb velocities, trends for axial climb and descent being related to the change in effective rotor inflow can be observed for the flutter onset. Since the effective inflow velocity only decreases slightly within climb flight, the rotor speed for flutter onset remains almost the same as found in hover flight. For the operation of the rotor at moderate descent velocities, the effective inflow velocity is increased and the relative flutter onset is found at a 3 % larger rotor speed than in hover flight. Here, the change of effective rotor inflow obtained is dominant, since it modifies torsion damping within the critical flutter coupling and influences the flutter onset depending on climb or descent flight, respectively.

1. INTRODUCTION

This paper summarizes the aeroelastic modelling and steps performed for a flutter assessment of the 7AD rotor model in steady axial flight utilizing a multibody system (MBS). The objective is the stability assessment of the elastic rotor blade using tight coupling between the multibody system and an unsteady aerodynamic model based on indicial functions [1] for rotor blade sections. The fast aerodynamic model has been developed at the DLR Institute of Aeroelasticity and used for the stability analyses of isolated rotor setups with straight [2] and double-swept rotor blades [3] in the DLR projects FAST- and URBAN-Rescue before test entry. Here, the use of indicial functions allows to separate unsteady aerodynamic effects related to blade airfoil, rotor inflow as well as rotor wake periodicity and to study their influence on flutter onset.

The 7AD rotor from Figure 1 was included in several European wind tunnel campaigns and operated as isolated or main rotor of a complete helicopter setup. Also, the GOAHEAD experimental setup [4] in the DNW-LLF wind tunnel made use of this articulated rotor. An earlier contribution [5] already dealt with the flutter assessment of the isolated 7AD rotor and the available MBS model formed the basis for the first application of the new unsteady aerodynamic model based on the extended Wagner function for axial rotor flow. So far, flutter assessment was limited to hover flight and it was found [6] that rotor inflow has major impact for the flutter onset of the rotor blade. Focus of this paper is to find out how flutter results change in steady axial flight for climb and descent.

Figure 1: 7AD isolated rotor in ONERA S1 wind tunnel.

In general, major improvement of the overall prediction capability for dynamic and aeroelastic simulation of rotorcraft is available by means of a multibody system for the setup of the dynamic model [7]-[8] which is characterized by connected rotary and non-rotary substructures. The application of multibody dynamics allows the consideration of all non-linear contributions relevant in a rotating system like geometric stiffening of the flexible blades and additional damping terms activated by gyroscopic effects as well as the provision of a correct mechanical interface between the rotating and non-rotating frames by applying non-linear joint definitions. Here, the multibody system SIMPACK [9]-[10] is used for the setup and simulation of the dynamic model of the 7AD rotor with its flexible blades. Flexibility of the non-rotating blade is described in the multibody system SIMPACK with a modal approach for available finite element models. For the assessment of the rotor in axial inflow condition, an unsteady theory using indicial aerodynamics based on the extended Wagner function in combination with steady two-dimensional airfoil data is applied to the multibody model. This approach allows an efficient and robust flutter assessment of DLR rotor setups in the design process and before entry into service, but is currently limited to axial flight considering hover, climb and descent.

2. NUMERICAL METHODS

2.1. Multibody Dynamics

The multibody system SIMPACK [9]-[10] is used to set up and simulate the dynamic model of the rotor with its flexible rotor blades including large rigid body motions of the rotor hub and blade hinges as well as small deformations of the elastic structure. The development of the simulation package was originally initiated by DLR and later out-sourced for further development and commercial distribution.

Flexibility of the non-rotating blade is described in the multibody system SIMPACK with a modal approach [11]-[12] for available finite element models. Several features allow the introduction of elastic rotor blades:

(A) Implementation of complete elastic blade as one elastic body and additional geometric stiffness terms via standard FlexModal interface

(B) Implementation of elastic blade with connected elastic substructures via standard FlexModal interface

(C) Application of the intrinsic elastic beam model SIMBEAM

(D) Application of the Rotor Blade Generator based on SIMBEAM

Feature (A) allows the straight-forward use of finite element models of industrial model size. Currently, the FlexModal interface supports ABAQUS, ANSYS, MSC.NASTRAN, NX.NASTRAN, PERMAS and RADIOSS. The feature (B) might be advantageous to add further non-linear characteristics of the multibody joints that interconnect elastic substructures. In addition, feature (C) and (D) provide a solution, if a finite element code is not available or is not supported by FlexModal. In the present work, SIMPACK 2021 has been used.

Feature (A) which is based on the implementation of the complete elastic model together with additional geometric stiffness using the FlexModal interface is chosen for the 7AD rotor blades. Two FEM solutions from a preprocessing step with the finite element code MSC.NASTRAN are required in order to process the blade:

- A modal solution provides the modal elastic model with natural frequencies and mode shapes for the non-rotating blade at Ω=0 rad/s.
- A static solution provides the geometric stiffness terms for the description in the relevant degrees-of-freedom of the rotating blade for Ω>0 rad/s (centrifugal forces due to angular velocity).

FlexModal reads the model geometry, mass and stiffness matrices, natural frequencies, mode shapes, geometric stiffening terms and the used load case entries for the derivation of the geometric stiffening terms from the pre-processed finite element data. Then, FlexModal translates this input into a common flexibility description which is based on the Standard Input Data (SID) format as described in [12]. The file containing the flexible substructure is added in SIMPACK with marker locations which are the same as found at the node positions in the finite element model, changing a rigid into an elastic body. Regarding aspects of component modal synthesis and substructuring, any hybrid model consisting of rigid and flexible bodies can be built. Rigid bodies can be made flexible by the introduction of a modal elastic model as described above or spring stiffness can be applied to a joint between two bodies from the MBS element library. SIMPACK adds the additional equations for the modal degrees-of-freedom to the set of differential algebraic equations (DAE) and solves the resulting set of equations.

2.2. Indicial Aerodynamics

An unsteady theory using indicial aerodynamics based on Wagner's function [1] in combination with steady two-dimensional airfoil data is applied to the multibody model. The fast aerodynamic model is based on radial independent strips and has been implemented using the approximation of R.T. Jones for Wagner's function [2]-[3]. This function considers a two-dimensional thin airfoil in impulsive motion from rest to uniform velocity and is commonly used as a model to describe the unsteady lift development for a change in angle-of-attack with fixed wing problems. According to Y.C. Fung [13], the description of unsteady lift is extended from an impulsive to a general motion including both, pitch and heave motion by considering unsteady apparent mass terms. All indicial response functions represent the circulatory parts of unsteady lift, are implemented in terms of a state space formulation as User Force Element (UFEL) in MBS SIMPACK and extended for rotors under axial flow condition. Related contributions include blade airfoil from the Wagner function [14], axial dynamic inflow from a non-linear differential equation [1] derived out of the results gained by Carpenter and Fridovich [15], and wake periodicity as modelled in Loewy's function [16]. All circulatory contributions are considered as dynamic states in the MBS.

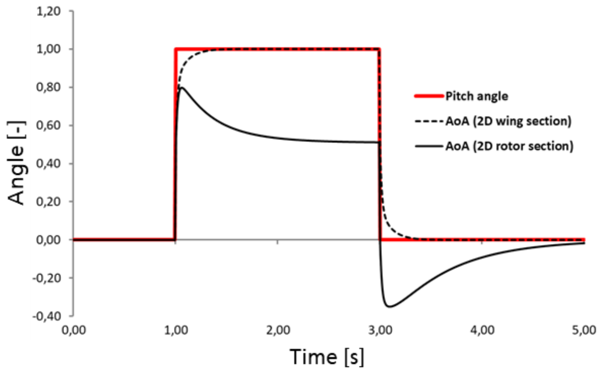

Figure 2: Temporal development of angle-of-attack (AoA) for pitch step input due to axial inflow dynamics.

The influence of added rotor inflow on the development of unsteady lift is obtained by applying pitch step excitations in the SIMPACK force element and evaluating the temporal development for the angle-of-attack which is a measure for lift and can be compared to the pitch input. Here, the indicial response for the Wagner function and axial dynamic inflow interacts depending on two separate scales for reduced time which is faster for the contribution from Wagner's function (rotor in-plane dynamics) and slower for axial inflow (rotor out-of-plane dynamics). As illustrated in Figure 2 for a two-bladed rotor, dynamic axial inflow reduces the effective angle-of-attack for the rotor section, whilst a wing section without inflow follows the basic Wagner function and reaches the commanded pitch angle. Hence, the onset of rotor inflow decreases the angle-of-attack towards a steady value which represents the so-called lift deficiency [17] of a rotor under axial inflow. To complete the extension of Wagner's function to axial rotor flow, the periodicity term from Loewy's function [16] is implemented in the state space model of the SIMPACK force element. The finalized model was carefully tested for harmonic pitch oscillation to gain aerodynamic transfer functions for comparison of the basic Wagner function with the extended models. As an example, Figure 3 shows the lift amplitudes and phase angles versus rotor harmonics for the radial section of a four-bladed rotor (f = 10 Hz, r = 1.0 m, b = 0.05 m, CT_0 = 0.008263) undergoing a harmonic pitch oscillation around mid chord. The influence of inflow and periodicity related to 4/rev can be clearly seen in both, lift amplitude and phase angle. For the chosen rotor parameters, 1/rev equals a reduced frequency of k = 0.05. Similar results with respective periodic content are obtained for a variation of the blade number as presented in [6] for the one-bladed rotor (where the plotted phase angle for both extensions needs a correction by factor 2·π).

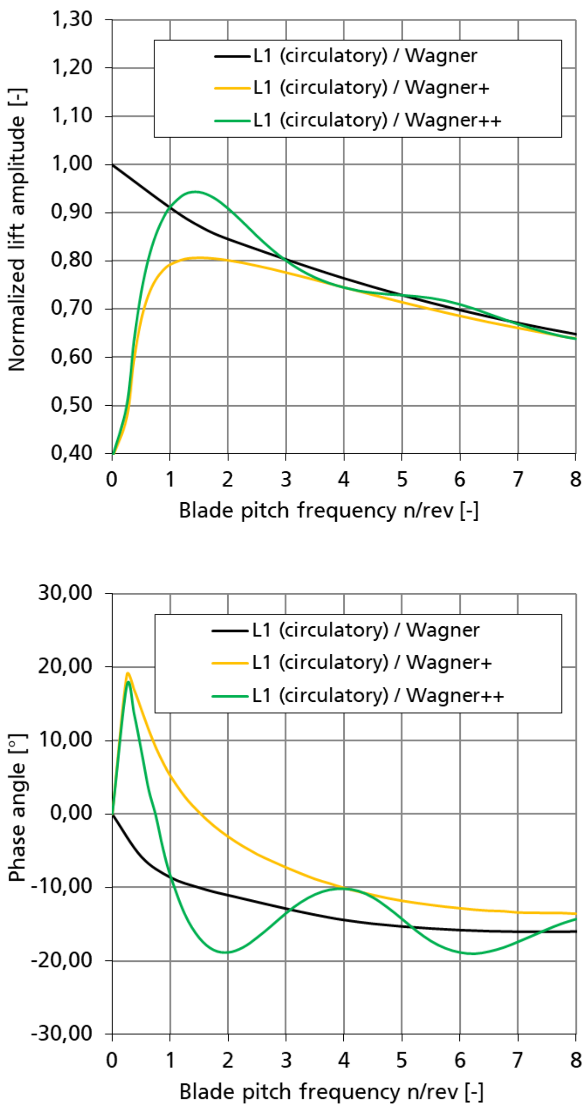

Figure 3: Unsteady lift amplitudes and phase angles of a four-bladed rotor obtained with Wagner function and extensions for rotor inflow (+) and wake periodicity (++).

2.3. Aeroelastic Assessment

Standard features in MBS SIMPACK allow the aeroelastic assessment in a tightly-coupled manner on equation level of the rotor blades for axial inflow condition in time domain and by using linearized results. The latter approach which is based on linearization, consecutive analysis of the eigenbehaviour and stability rating from damping values can be followed here, since the system matrices for the symmetric rotor with axial inflow remain time invariant and the unsteady aerodynamic forces are considered in the dynamic state set. The analysis is performed with the intrinsic eigensolver and delivers typical flutter results in terms of frequency and damping plots. In general, these allow the verification of frequency placement and stability for the aeroelastic rotor system.

3. MODELS AND RESULTS

3.1. Dynamic and Aerodynamic Models

The dynamic setup of the 7AD rotor system is depicted in Figure 4 and consists of the flexible rotor blades and a rigid model for the DLR-ONERA rotor hub that is improved with measured values [18] for pitch link and lagging spring stiffness as well as lagging damping. The rotor hub is modelled with SIMPACK features to close the kinematic loop comprising of lead-lag hinge, flap hinge and pitch bearing via the pitch link to the swash plate. The flexibility of the non-rotating blade is described in the multibody system with a modal approach from a real modes solution and additional geometric stiffness contributions for the rotating blade are considered by static load cases for the relevant degrees of freedom, both computed in a pre-processing step with the finite element software MSC.NASTRAN. Further, the centrifugal pitching moment is considered at each radial marker via a SIMPACK Expression.

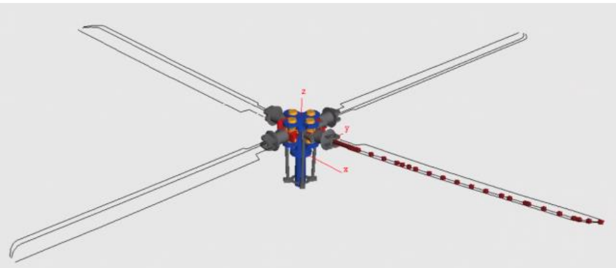

Figure 4: Multibody model of articulated 7AD rotor.

The four bladed rotor has a diameter of 4.2 m, mean blade chord of 0.14 m and a solidity of 0.085. Both blade hinges are located at a radius of 0.075 m and the blade attachment is found at the radial station of 0.275 m. The blade mass is approximately 3.18 kg. Figure 5 shows the MSC.NASTRAN beam model of the 7AD rotor blade along the straight blade axis and curved blade tip with additional rigidly connected nodes to model trailing and leading edge positions for spatial coupling.

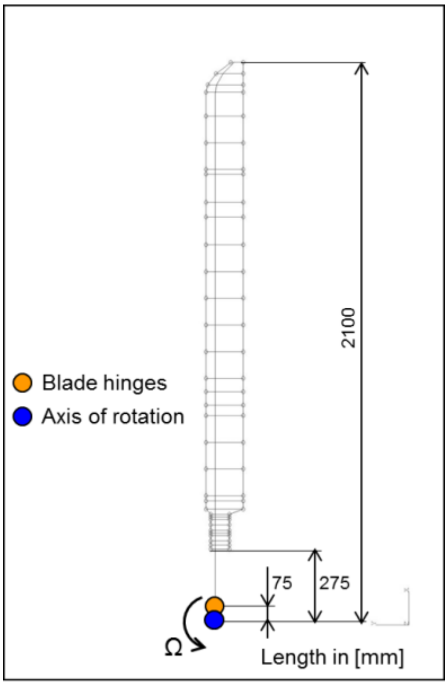

Figure 5: Finite element model with rigidly connected leading and trailing edge.

As described earlier by the author [5], measured vibration data is available from a ground vibration test (GVT) with rowing hammer technique for the clamped blade comprising modal properties in terms of natural frequencies and mode shapes for the non-rotating 7AD rotor blade. The comparison of simulation results for the clamped beam model with the experimental modal data takes the measured frequencies into account and global stiffness parameters of the finite element models are adjusted with respect to modulus of elasticity and shear, if necessary. The natural frequencies for the elastic blade modes obtained with the finite element and multibody model are given in Table 1 in terms of a relative frequency deviation with respect to the GVT results as reference values.

Mode	f_{GVT} [-]	f_{FEM} [-]	f_{MBS} [-]
1 / F1	1.000	0.980	0.980
2 / L1	1.000	1.009	1.009
3 / F2	1.000	1.015	1.015
4 / F3	1.000	0.991	0.991
5 / T1	1.000	0.996	0.996
6 / F4	1.000	1.034	1.034
7 / L2	1.000	1.062	1.062
8 / F5	1.000	1.004	1.004
9 / F6	1.000	0.995	0.995
10 / T2	1.000	0.959	0.959
(F = flap mode / L = lag mode / T = torsion mode)			

Table 1: Comparison of calculated frequencies with GVT data for clamped rotor blade.

Each rotor blade is equipped with 34 SIMPACK User Force Elements along the straight blade axis and the parabolic tip section. They provide the unsteady aerodynamic forces from circulation based on the extended Wagner function and related non-circulatory enhancements for the general motion of the airfoil section taking heave and pitch into account. The unsteady aerodynamic contributions from circulation include blade airfoil (1), axial rotor inflow (2) and wake periodicity (3) from rotor blade interaction. Here, indicial functions allow to separate these effects into three cases according to Table 2 and to study their individual impact on rotor blade flutter. Similar to earlier aeroelastic assessments of the 7AD rotor [5]-[6], a pitch setting according to a blade thrust of 827 N at nominal rotor speed is chosen for the test cases.

Case	1 / Wagner	2 / Wagner+	3 / Wagner++
Blade airfoil	x	x	x
Rotor inflow		x	x
Wake periodicity			x

Table 2: Settings for unsteady aerodynamic model.

3.2. Dynamic Simulation Results

The dynamic simulation results for hover [6] are gained from the application of linearization features in MBS SIMPACK and show the development of the rotor frequencies versus nominal rotor speed for the dynamic rotor setup. Since the rotor system remains unaccelerated for steady axial flight, the dynamic results for hover can be also referenced for constant climb and descent speeds. As preparatory steps, an equilibrium computation for the derivation of the dynamic model states followed by a preload computation are performed to adjust the rotor model to the chosen rotor speed.

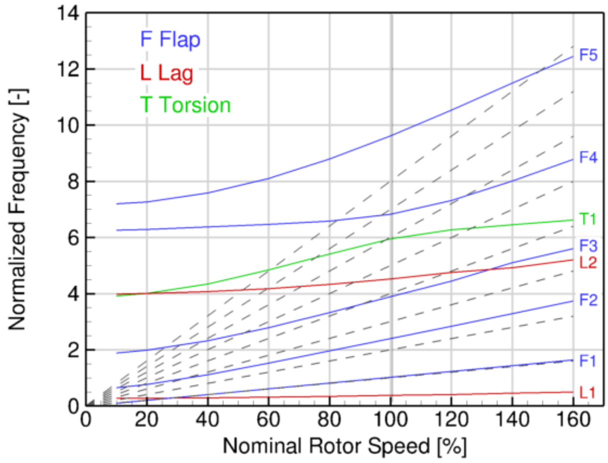

Figure 6: Rotor frequencies for the dynamic model.

The normalized frequencies of the 7AD rotor are found in Figure 6 and correlate well with other results [19] available inside DLR. Here, the plotted modes are numbered in ascending frequency order and the colour code describes the major motion contribution in terms of blade lag (red), flap (blue) and torsion (green) at nominal rotor speed of 100 %. Hence, the mode assigned as first elastic torsion T1 represents the flap bending mode F4 for rotor speeds below the nominal operation speed, and vice versa. The dashed lines show the rotor harmonics up to 8/rev and allow the verification of the frequency placement for the 7AD dynamic rotor setup.

3.3. Aeroelastic Simulation Results

Simulation results in Figure 7 and Figure 8 show the 7AD flutter diagrams for hover flight [6] and represent Case 1 and Case 2/3 from Table 2, respectively. The flutter diagrams summarize the development of rotor blade frequencies and natural damping of the modes versus nominal rotor speed for the aeroelastic system using Wagner's function and circulatory extensions together with the non-circulatory contributions from apparent mass. In general, both curves allow the verification of frequency placement and stability for the aeroelastic rotor system. Again, they are processed using available SIMPACK linearization features together with two preceding simulation steps to derive an equilibrium for all dynamic states including indicial aerodynamics and then to preload the rotor with the appropriate aerodynamic and centrifugal loads for the chosen rotor speed. Here, the unsteady motion parts from the SIMPACK User Force Element are considered by aerodynamic lag states which are found as real parts in the linearization result and thus, influence the

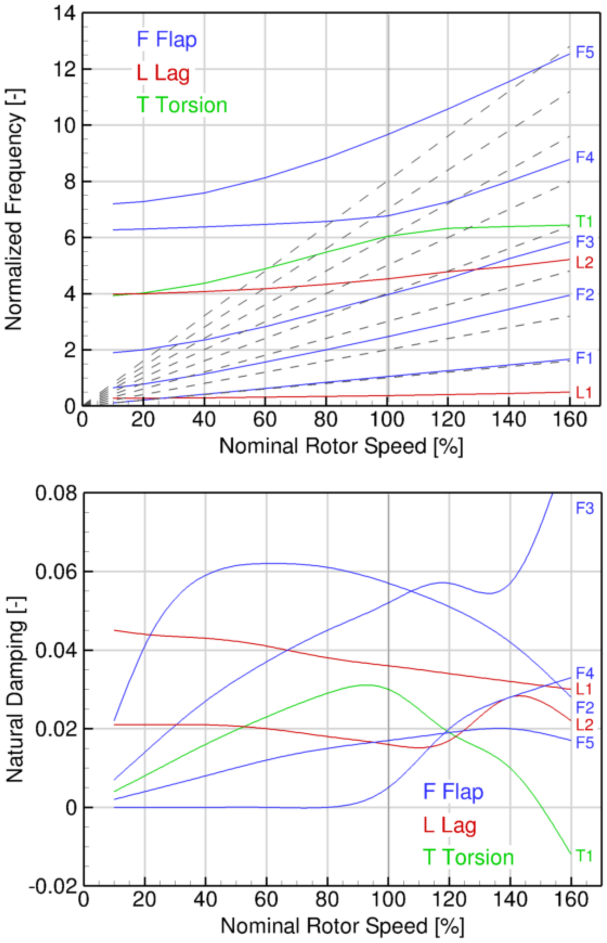

Figure 7: Rotor frequencies and damping for the aeroelastic model in hover (Case 1: Wagner).

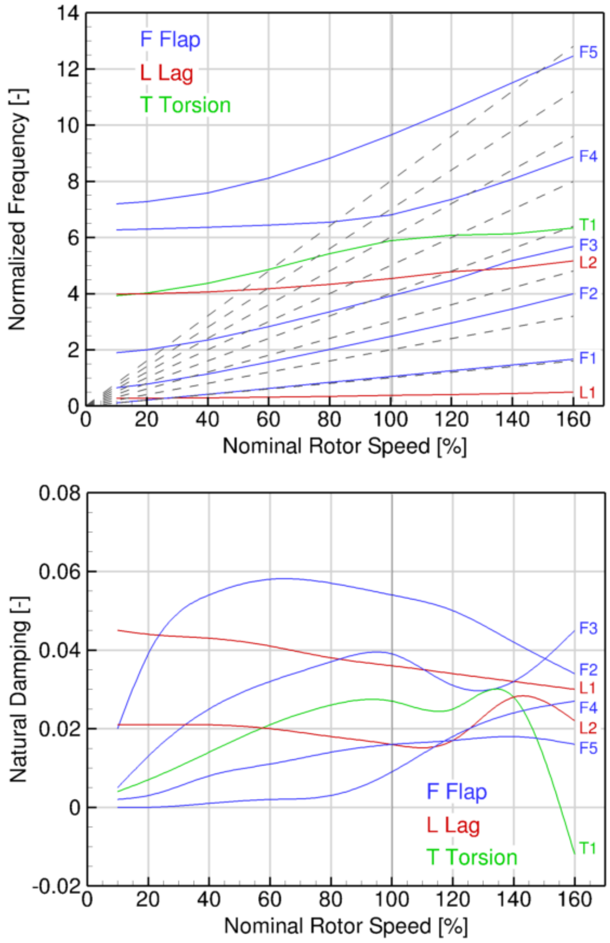

Figure 8: Rotor frequencies and damping for the aeroelastic model in hover (Case 2/3: Wagner+/++).

blade damping. As mentioned before, the dynamic rotor setup includes a measured value for lagging damping which introduces the large damping found with both lead-lag modes L1 and L2.

It was found and discussed earlier [6] that the consideration of rotor inflow (Case 2) shows a major impact on flutter of the 7AD rotor blade in hover flight, whilst added wake periodicity (Case 3) does not further change the flutter onset. The damping curves for all three cases indicate a classical bending-torsion coupling of the third flap mode F3 and the first torsion mode T1 as known for articulated rotor blades. This mode pair becomes instable at a nominal rotor speed of 151 % for Case 1 and 158 % for Case 2/3, respectively. Similar to the frequency curves of F4 and T1, the damping values for flap bending mode F4 represent those of torsion T1 below the nominal operation speed, and vice versa. In addition, a slight coupling is found between flap mode F3 and lead-lag mode L2 starting around the nominal rotor speed of 120 % which remains stable.

Now, the focus is to investigate the flutter onset for steady axial flight and compare it with hover flight. This requires the extension of the unsteady aerodynamic model Wagner++ to consider the influence of climb and descent velocities V_c on the induced velocity v_i due to rotor inflow. According to momentum theory [1], steady axial flight of an isolated rotor is related to the same thrust condition as found in hover flight and hence, the required thrust equals the overall weight for all three flight states. To perform a steady climb or descent, the overall mass flow through the rotor disc is increased by the climb velocity ($V_c > 0$) or decreased by the descent velocity ($V_c < 0$), respectively. The effective induced velocity v_i due to rotor inflow is derived from the induced velocity in hover flight v_h, which is known from the dynamic inflow model in the extended Wagner function, and follows as:

$$\text{(1)} \qquad \frac{v_i}{v_h} = -\left(\frac{V_c}{2\cdot v_h}\right) - \sqrt{\left(\frac{V_c}{2\cdot v_h}\right)^2 - 1}$$

(descent flight, valid for: $V_c / v_h \leq -2$)

(2) $$\frac{v_i}{v_h} = 1.0 - 1.125 \cdot \left(\frac{V_c}{v_h}\right) - 1.372 \cdot \left(\frac{V_c}{v_h}\right)^2 - 1.718 \cdot \left(\frac{V_c}{v_h}\right)^3 - 0.655 \cdot \left(\frac{V_c}{v_h}\right)^4$$

(descent flight, valid for: $-2 \leq V_c / v_h \leq 0$)

(3) $$\frac{v_i}{v_h} = -\left(\frac{V_c}{2 \cdot v_h}\right) + \sqrt{\left(\frac{V_c}{2 \cdot v_h}\right)^2 + 1}$$

(climb flight, valid for: $V_c / v_h \geq 0$)

The three equations are implemented in the SIMPACK User Force Element (UFEL) and Figure 9 illustrates the induced velocity ratio v_i/v_h versus climb velocity ratio V_c/v_h which corresponds to literature [1]. Here, the climb flight is related to a positive climb velocity ratio and leads to a decrease of effective induced velocity v_i, whilst increased values are found for descent at moderate descent velocities.

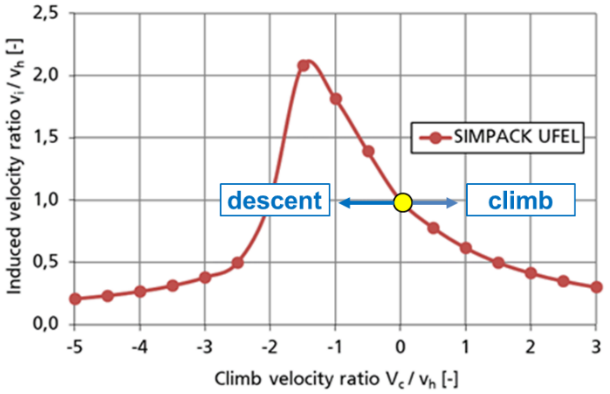

Figure 9: Induced velocity ratio for axial flight.

For the investigated axial flight velocities ranging from -6 to +6 m/s, climb velocity ratios between ±0.6 are found for the 7AD rotor with a thrust of 827 N per blade and a resulting rotor inflow of around 10 m/s. Hence, the investigated cases for climb flight are performed for a reduced and those for descent flight for an increased effective inflow, respectively. The comparability of flutter results for hover and axial flight requires the same blade thrust to fulfill the assumption of steady flight. To reach this condition for the three operational modes, the blade pitch is adjusted to obtain the required thrust value for the nominal rotor speed of 100 %. During the variation of rotor speed in the flutter analysis, the pitch setting remains unaltered what leads to a more or less constant thrust coefficient of approximately 0.0043.

As for the hover reference case from Figure 8, the flutter assessment of Case 3 (Wagner++) is performed within the above mentioned axial flight velocity range in steps of 2 m/s considering a variation of nominal rotor speed between 10 % and 160 % and beyond, if required to find blade flutter. For all studied axial flight velocities, the known flutter coupling of flap bending mode F3 and torsion mode T1 from hover remains. According results for climb and descent are summarized in terms of a relative flutter onset taking hover as reference into account and shown in Figure 10.

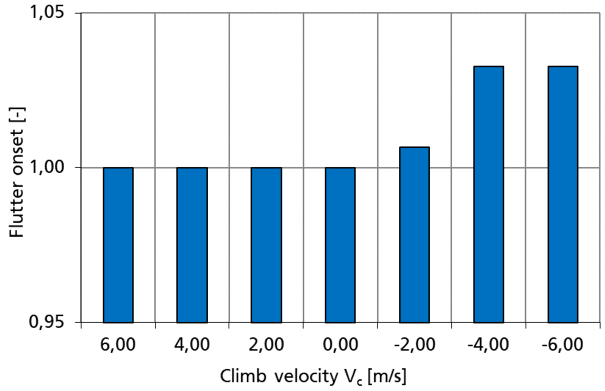

Figure 10: Relative flutter onset for 7AD rotor blade in axial flight (Case 3: Wagner++).

Within the studied range of climb velocities, trends for axial climb and descent which are related to the change in effective rotor inflow can be observed for the flutter onset of the articulated 7AD rotor blade. Since the effective inflow velocity v_i is slightly decreased within climb flight, the rotor speed for flutter onset remains the same as found in hover flight. For a further increase of climb velocity V_c beyond the studied values, a small reduction of rotor speed for flutter onset might occur. For the operation of the rotor in descent flight at moderate descent velocities V_c, the effective inflow velocity v_i is increased and the relative flutter onset is found at a 3 % larger rotor speed than in hover flight. Here, the change of effective rotor inflow obtained in axial flight is dominant, since it modifies torsion damping within the critical flutter coupling and influences flutter onset depending on climb or descent flight, respectively.

4. CONCLUSIONS AND OUTLOOK

The 7AD rotor blade has been assessed for flutter stability in steady axial flight. For the aeroelastic analyses, the multibody model was tightly-coupled with an unsteady aerodynamic model based on the extended Wagner function and related enhancements for the general motion of an airfoil section considering heave and pitch. So far, the mathematical setup of the extended Wagner function in state space considered unsteady aerodynamic contributions related to the blade airfoil as well as rotor inflow and wake periodicity for axial flow in hover flight. A correction to obtain the effective rotor inflow in climb and descent extends the applicability now to steady axial flight.

As known for articulated rotor blades, the straight 7AD blade with parabolic blade tip shows the classical bending-torsion coupling which remains for all studied axial flight velocities. Here, comparability of flutter results for hover and axial flight requires the same blade thrust to fulfill the assumption of steady axial flight. As for the hover reference case, the flutter assessment of the articulated 7AD rotor blade is performed considering a variation of nominal rotor speed. According results for climb and descent are evaluated in terms of a relative flutter onset taking hover as reference into account. Within the studied range of climb velocities, trends for axial climb and descent being related to the change in effective rotor inflow can be observed for the flutter onset. Since the effective inflow velocity only decreases slightly within climb flight, the rotor speed for flutter onset remains almost the same as found in hover flight. For the operation of the rotor in descent flight at moderate descent velocities, the effective inflow velocity is increased and the relative flutter onset is found at a 3 % larger rotor speed than in hover flight. Here, the change of effective rotor inflow obtained in axial flight is dominant, since it modifies torsion damping within the critical flutter coupling and influences flutter onset depending on climb or descent flight, respectively.

The presented approach based on the extended Wagner function is fast and robust. It allows for an initial flutter analysis and will be implemented into an existing process chain for rotor blade optimization to introduce flutter checks at an early design stage.

5. REFERENCES

[1] Leishman JG. Principles of Helicopter Aerodynamics. Cambridge University Press, New York, 2nd edition, Chapter 8, 2000.

[2] Arnold J, Waitz S. Using Multibody Dynamics for the Stability Assessment of a New Rotor Test Rig. 43rd European Rotorcraft Forum, Milan, 2017.

[3] Arnold J, Waitz S. Using Multibody Dynamics for the Stability Assessment of a New Double-Swept Rotor Blade Setup. 44th European Rotorcraft Forum, Delft, 2018.

[4] Schwarz T, Pahlke K. CFD code validation for complete helicopters - The European GOAHEAD project. 67th American Helicopter Society Forum, Virginia Beach, Virginia, 2011.

[5] Arnold J. Flutter Assessment of a Rotor Blade with Innovative Layout in Hover using Indicial Aerodynamics. 72nd American Helicopter Society Forum, West Palm Beach, Florida, 2016.

[6] Arnold, J. Flutter Assessment of a Rotor Blade in Hover Based on Indicial Aerodynamics Considering Blade Profile, Rotor Inflow and Wake Periodicity," 47th European Rotorcraft Forum, Glasgow (virtual), 2021.

[7] Morillo J, Singh R, Wasikowski M. Model Development and Integration of DYMORE at Bell Helicopter. 64th American Helicopter Society Forum, Montréal, 2008.

[8] Waitz S. The structural dynamics of a free flying helicopter in MBS- and FEM-analysis. 39th European Rotorcraft Forum, Moscow, 2013.

[9] Lugner P, Arnold M, Vaculin O (Eds). Vehicle System Dynamics (Special issue in memory Professor Willi Kortüm), Vol. 41, No. 5, 2004.

[10] https://www.3ds.com/products-services/simulia/products/simpack/

[11] Schwertassek R, Wallrapp O. Dynamik flexibler Mehrkörpersysteme. Vieweg, 1999.

[12] Wallrapp O. Standardization of Flexible Body Modeling in Multibody System Codes, Part I: Definition of Standard Input Data, Mechanics of Structures and Machines, 22(3), pp. 283-304, 1994.

[13] Fung YC. An Introduction to the Theory of Aeroelasticity. Dover Publications Inc, New York, 1993, Chapter 6.

[14] Wagner H. Über die Entstehung des dynamischen Auftriebes von Tragflügeln, Zeitschrift für angewandte Mathematik und Mechanik, Band 5, Heft 1, 1925.

[15] Carpenter PJ, Fridovich B. Effect of a Rapid Blade Pitch Increase on the Thrust and Induced Velocity Response of a Full-Scale Helicopter Rotor. NACA TN 3044, 1953.

[16] Loewy RG. A Two-Dimensional Approximation to the Unsteady Aerodynamics of Rotary Wings. Journal of the Aeronautical Sciences, Vol. 24, No. 2, pp. 81-92, 1957.

[17] Miller RH. Rotor Blade Harmonic Air Loading. AIAA Journal, Vol. 2, No. 7, 1964.

[18] Hoffmann F, Opitz S. Documentation for AT4 Structural Properties. Version 1.1, DLR Institute of Flight Systems, 2010.

[19] Surrey S, Wendisch JH, Wienke F. Coupled fluid-structure simulations of a trimmed helicopter rotor in forward flight. Proc 19th DGLR symposium STAB, Munich, 2014.